ADVANCED ENERGY MATERIALS
www.advenergymat.de

Enhanced Efficiency Parameters of Solution-Processable Small-Molecule Solar Cells Depending on ITO Sheet Resistance

*Dong Hwan Wang, Aung Ko Ko Kyaw, Vinay Gupta, Guillermo C. Bazan, and Alan J. Heeger**

Bulk-heterojunction (BHJ) solar cells based on phase-separated blends of organic materials of donor and acceptor (fullerene derivative) have been in continuous development over the past two decades.[1–8] Recently, solution-processable small molecule-based BHJ solar cells exhibiting comparable power conversion efficiency of near 8% to the polymers with high potential under simple and optimized processing conditions.[9–13] The small-molecule donors have attractive features, including relatively simple synthesis and purification steps, mono-dispersity, and improved batch-to-batch reproducibility.[14]

Indium tin oxide (ITO) substrates have been widely used for BHJ solar cells because of their high transparency and excellent conductivity. There are several promising transparent conducting oxides (TCOs) that may replace ITO, having potentially better properties for use as anode materials and in order to implement flexibility for the next generation of opto-electronic devices. Organic films are being developed using carbon nanotubes (CNT)[15,16] and graphene,[17–19] which have the combined advantages of high transparency in the infrared and high conductivity. Also, the solution-processable poly(3,4-ethylenedioxythiophene) poly(styrenesulfonate) (PEDOT:PSS) is used as the anode material, deposited via spin-casting several times, to increase the conductivity.[20–22] However, the losses in BHJ solar cells with organic anode materials yield lower power conversion efficiencies (PCE) than devices with ITO because of the high sheet resistance of the substrate (causing reduced J_{SC} and reduced fill factor (FF)). Therefore, selection of the best ITO substrate is one of the important factors to get high performance solar cells.

Here, we have fabricated efficient solution-processable small-molecule solar cells with PCE of 8.24% from a 7,7′-(4,4-bis(2-ethylhexyl)-4H-silolo[3,2-b:4,5-b′]dithiophene-2,6-diyl)bis(6-fluoro-4-(5′-hexyl-[2,2′-bithiophen]-5-yl)benzo[c][1,2,5]thiadiazole) (p-DTS(FBTTh$_2$)$_2$): [6,6]-phenyl C$_{71}$-butyric acid methyl ester (PC$_{71}$BM) BHJ with enhanced J_{SC} and FF using a low sheet resistance of ITO (5 Ω/□) substrate. The increased $J_{SC}$and FF originate from the reduced series resistance (R_s).

The device architecture and the molecular structures of p-DTS(FBTTh$_2$)$_2$ and the acceptor of PC$_{71}$BM are shown in **Figure 1**. The devices are fabricated on glass/ITO (100–450 nm) with subsequent deposition of PEDOT:PSS (ca. 30 nm), BHJ (ca. 100 nm), and Ca (20 nm) capped with Al (80 nm). The ITO substrates were selected with three different sheet resistances, 5, 20, and 40 Ω/□ to characterize the effect of the ITO sheet resistance (and transparency) on J_{SC}, FF, and PCE. The thickness of ITO is directly related to the the sheet resistance. Therefore, the 5, 20, and 40 Ω/□ sheet resitances were confirmed by measurement of the ITO thickness using a surface profiler, giving values of 450, 150, and 100 nm, respectively. Figure 1b shows the energy level diagrams of all the deposited layers. The highest occupied molecular orbital (HOMO) and lowest unoccupied molecular orbital (LUMO) energy levels of p-DTS(FBTTh$_2$)$_2$ are −5.12 and −3.34 eV, respectively.[12,13]

Figure 2 shows the transmittance of the ITO substrates with sheet resistances of 5, 20, and 40 Ω/□ as a function of wavelength. From this result, the 40 Ω/□ ITO exhibits 80% transmittance over the spectral region from 450 to 750 nm. Thus, the higher surface resistance solar cells will introduce significant loss from absorption (see Figure 2) in the BHJ layer because the p-DTS(FBTTh$_2$)$_2$ and PC$_{71}$BM BHJ absorption spectra are maximum within the wavelength regime from 400 to 700 nm.[12,13] Herein, we observed that thin ITO does not necessarily lead to an increase in the optical transmittance of the film, probably due to the interference of light inside the thin film, the thickness of which is comparable to the wavelength of the light. The color of ITO substrate appears slightly different depending on thickness and sheet resistances from bright green (5 Ω/□) to bright purple (40 Ω/□), as shown in the inset in Figure 2.

To characterize the efficiency parameters of the solution-processable small-molecule p-DTS(FBTTh$_2$)$_2$:PC$_{71}$BM BHJ solar cells, we fabricated devices using different ITO sheet resistances (5, 20, and 40 Ω/□). As shown in **Figure 3**a, the device with 40 Ω/□ ITO sheet resistance exhibits a PCE of 5.94% from the following parameters: V_{oc} = 0.797 V, J_{SC} = 13.54 mA cm^{-2}, and FF = 55. On the other hands, the solar cells with 20 Ω/□ ITO sheet resistance show improved PCE = 7.58% with V_{oc} = 0.784 V, J_{SC} = 14.33 mA cm^{-2}, and FF = 67.5. Finally, solar calls using the 5 Ω/□ ITO sheet resistance yield PCE = 8.24% with

Dr. D. H. Wang,[+] Dr. A. K. K. Kyaw,[+] Prof. G. C. Bazan, Prof. A. J. Heeger
Center for Polymers and Organic Solids
University of California at Santa Barbara
Santa Barbara, California 93106-5090, USA
E-mail: ajhe1@physics.ucsb.edu
Dr. V. Gupta
Organic and Hybrid Solar Cell Group
CSIR- National Physical Laboratory
Dr. K. S. Krishnan Marg, New Delhi, 110012, India
[+] D.H.W and A.K.K.K contributed equally to this work.

DOI: 10.1002/aenm.201300277

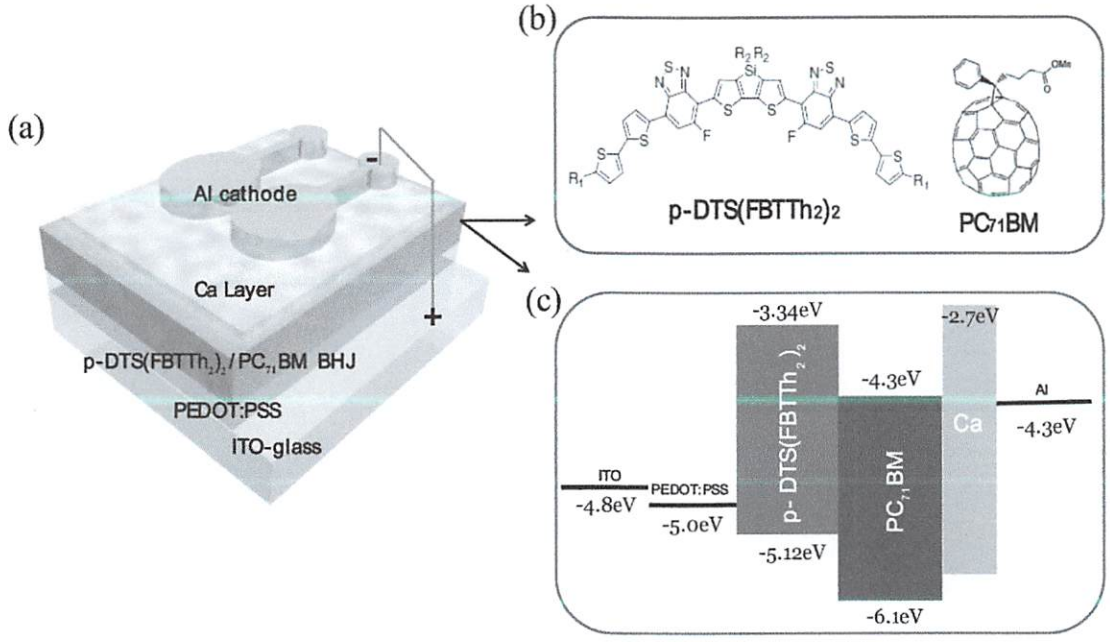

Figure 1. a) Device schematic of p-DTS(FBTTh$_2$)$_2$/PC$_{71}$BM BHJ solar cells. b) Molecular structure of p-DTS(FBTTh$_2$)$_2$ and PC$_{71}$BM. c) Band diagram levels of the device structure.

V_{oc} = 0.773 V, J_{SC} = 14.74 mA cm^{-2}, and FF = 72.4, respectively. These data are summarized in **Table 1**.

Figure 3b shows the EQE, which corresponds to the *J–V* curve of the devices in Figure 3a. The EQE value approaches 80% from 600 to 650 nm for the devices with a 5 Ω/□-ITO and enhanced J_{SC} of 14.74 mA cm^{-2}. In contrast, the EQE values of the devices having 20 and 40 Ω/□-ITO displayed lower values of 75% and 70%, respectively, near 600 nm, due to the reduced J_{SC} (14.33 and 13.54 mA cm^{-2}, respectively). The J_{SC} calculated for the device with a 5 Ω/□-ITO from the integration of EQE spectrum from 300 to 800 nm is 14.95 mA cm^{-2}, in a good agreement with the measured J_{SC} of 14.75 mA cm^{-2} (approx. 1.4% error) obtained from the *J–V* curve, as shown in Table S1 in the Supporting Information. The nano-morphology of the p-DTS(FBTTh$_2$)$_2$:PC$_{71}$BM BHJ is independent of the ITO surface resistance, as confirmed by atomic force microscopy (AFM). The donor and acceptor exhibit nanoscale phase separation and long fibrillar structures, as shown in Figure S1 (the AFM scan size is 10 μm ×10 μm).

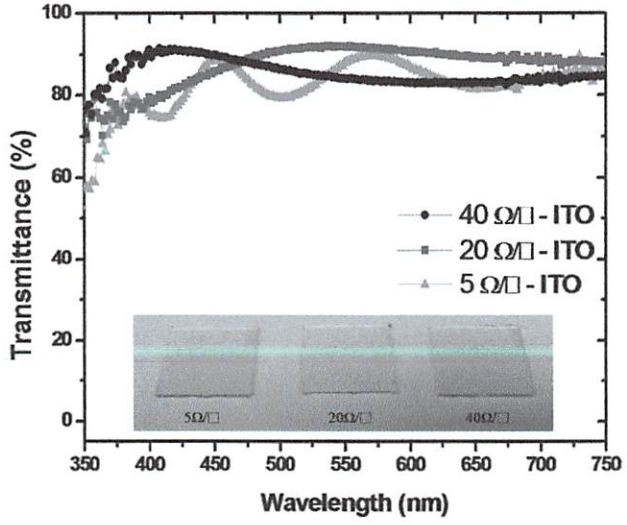

Figure 2. Transmittance (%) of the ITO substrates with sheet resistances of 5, 20, and 40 Ω/□ as a function of wavelength. The inset shows real images of the ITO having 5, 20, and 40 Ω/□.

In addition, the fill factor values of the p-DTS(FBTTh$_2$)$_2$:PC$_{71}$BM BHJ solar cells are critically related to the different ITO sheet resistance. The dependence of the PCE and FF on ITO sheet resistance are shown in **Figure 4**a. The device with a 5 Ω/□-ITO shows enhanced PCE of 8.24% and FF of 72.4%, significantly higher than the FF values obtained from the devices fabricated on 20 and 40 Ω/□-ITO. The high FF of the 5 Ω/□-ITO device has an increased shunt resistance, R_{sh} = 1.47 kΩ cm^2, and a reduced series resistance, R_s = 0.9 Ω cm^2. For the device with 20 Ω/□-ITO, R_{sh} = 1.27 kΩ cm^2 and R_s = 2.7 Ωcm^2, while the 40 Ω/□-ITO device has R_{sh} = 0.44 kΩ cm^2 and R_s = 13.09 Ω cm^2, as shown in the *J–V* curves obtained in the dark (see Figure 4b and Table 1). Therefore, the PCE of the devices from small molecule-based BHJ solar cells are correlated to the ITO sheet resistance because the efficiency parameters of the photocurrent density (J_{SC}) and fill factor (*FF*) are affected by the R_{sh} and R_s of the devices. It is well understood that the R_s of a solar cell depends on the resistance of the individual layers in the cell and contact resistance between adjacent layers. Hence, we also observed that R_s decreases with reduced sheet resistance of ITO. Unexpectedly, R_{sh} also increases with decreasing sheet resistance of ITO in our fabricated devices.

Adv. Energy Mater. 2013,
DOI: 10.1002/aenm.201300277

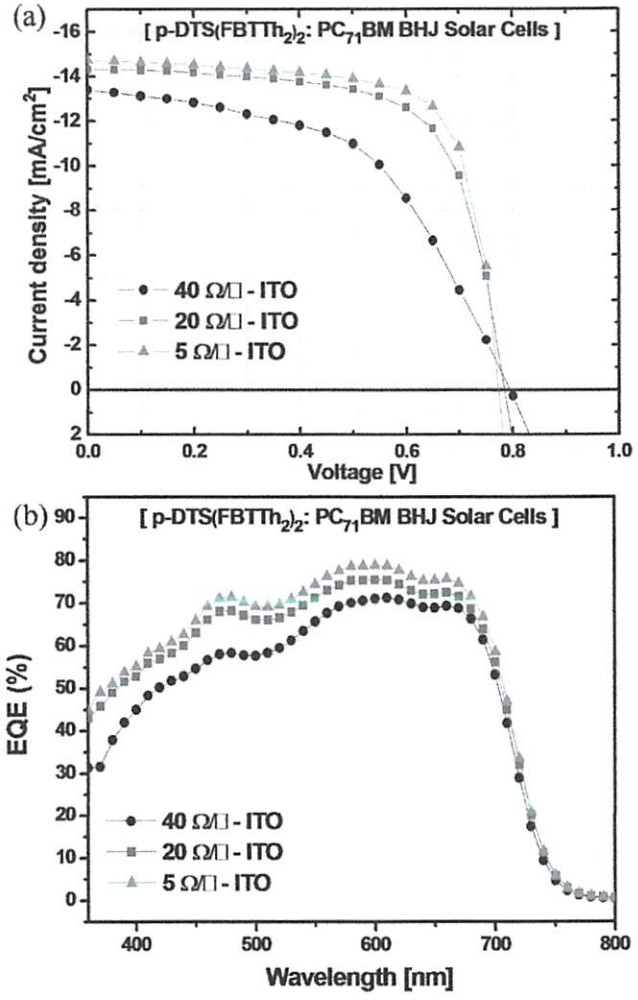

Figure 3. a) J–V characteristics of the p-DTS(FBTTh$_2$)$_2$/PC$_{71}$BM BHJ solar cells on ITO with sheet resistances of 5, 20, and 40 Ω/□ under AM 1.5G irradiation at 100 mW cm^{-2}. b) EQE spectra of the same devices.

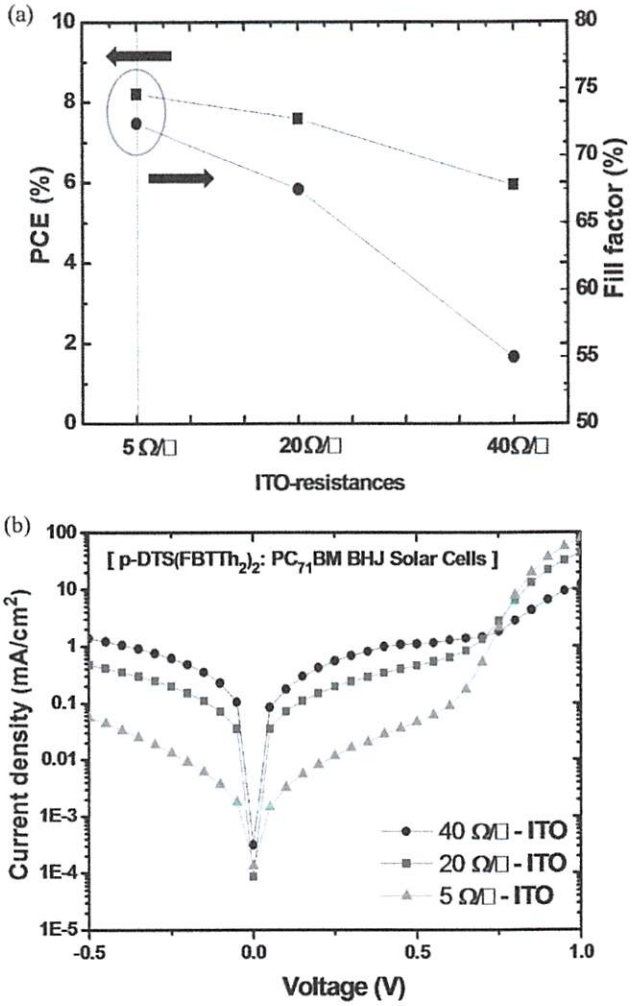

Figure 4. a) PCE (squares) and FF (circles) for devices with ITO sheet resistances of 5, 20, and 40 Ω/□. b) J–V characteristics of the p-DTS(FBTTh$_2$)$_2$/PC$_{71}$BM BHJ solar cells fabricated on ITO sheet with resistances of 5, 20, and 40 Ω/? as obtained in the dark.

The role of sheet resistance in increasing R_{sh} (also suppressing the leakage dark current in reversed bias) is not clear at that point and detailed studies are required to fully understand it.

One might speculate that the increase in J_{SC} is due to the optical interference effect which stems from the different thickness of ITO. Therefore, we calculated the optical electric field (E) distribution for a single wavelength illumination (600 nm, the maximum absorption peak of p-DTS(FBTTh$_2$)$_2$:PC$_{71}$BM) in the devices with different ITO thicknesses using the transfer matrix method proposed by Pettersson et al.[23] The simulation results show that the normalized modulus squared of the optical electric field $|E|^2$ is almost the same inside the BHJ layer for the different thicknesses of ITO (**Figure 5**). Therefore, the increase in J_{SC} of the device with a 5 Ω/□-ITO can be attributed to the enhanced charge collection of ITO with low sheet resistance, rather than the optical interference effect.

Finally, we checked the reproducibility of the PCE and FF values by fabricating several independent devices on ITO with different sheet resistances as shown in Figure S2 (see the Supporting Information). Another positive effect for the device with a 5 Ω/□-ITO is that the FF and PCE are similar values, with narrow variations between minima and maxima of 72.2% to 72.8%, and 8.00% to 8.24%, respectively. The device with a 5 Ω/□-ITO shows average FF value of 72.4%, with an average PCE of 8.10%, based on the inset of Figure S2.

Table 1. The efficiency parameters of the solution - processable small - molecule solar cells from a p-DTS(FBTTh$_2$)$_2$/PC$_{71}$BM BHJ obtained from ITO with various sheet resistances.

ITO sheet resistance	V_{oc} [V]	J_{SC} [mA cm^{-2}]	FF [%]	PCE [%]	R_s [Ω cm^2]	R_{sh} [kΩ cm^2]
40 Ω/□	0.797	13.54	55.0	5.94	13.09	0.44
20 Ω/□	0.784	14.33	67.5	7.58	2.7	1.27
5 Ω/□	0.773	14.74	72.4	8.24	0.9	1.47

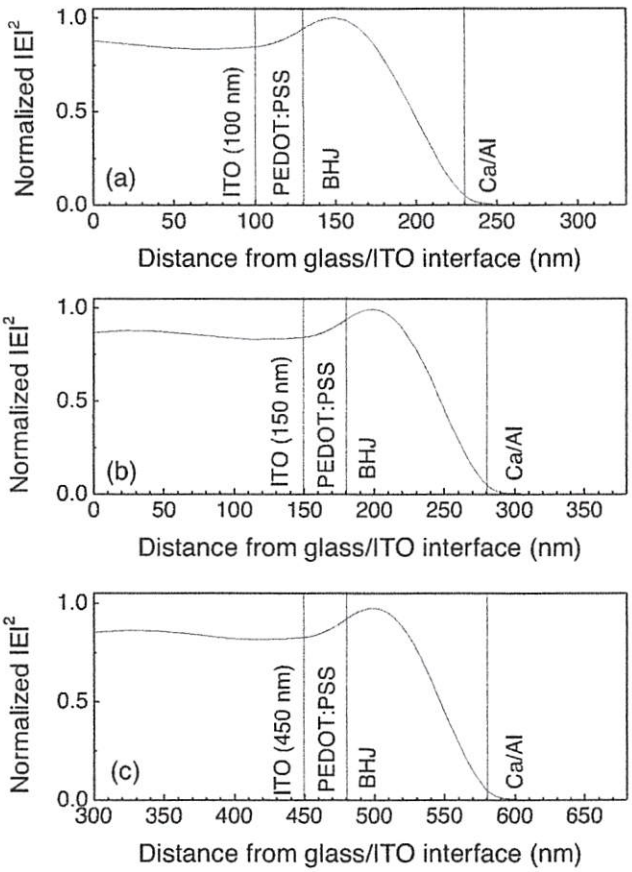

Figure 5. The simulated distribution of the normalized modulus squared of the optical electric field $|E|^2$ inside the devices with different thicknesses of ITO: a)100, b) 150, and c) 450 nm for a wavelength of 600 nm, where the maximum abosrption peak of p-DTS(FBTTh$_2$)$_2$/PC$_{71}$BM BHJ is located.

In summary, we fabricated solution processable small molecule solar cells from the p-DTS(FBTTh$_2$)$_2$:PC$_{71}$BM BHJ using a 5 Ω/□-ITO sheet resistance substrate (ITO thickness thickness of 450 nm) which exhibits transmittance of 90% at 550 nm. The PCE = 8.24% for solar cells fabricated on 5 Ω/□-ITO with J_{SC} = 14.74 mA/cm^2, and FF = 72.4% significantly higher than obtained from cells fabricated on 20 Ω/□-ITO and a 40 Ω/□-ITO, respectively. The PCE and FF are reproducible based on the 5 Ω/□-ITO due to the enhanced R_{sh} and the reduced R_s. Using the 5 Ω/□-ITO, the average PCE = 8.10%.

Experimental Section

Fabrication of SM-BHJ Solar Cells (p-DTS(FBTTh$_2$)$_2$/PC$_{71}$BM): Films with different sheet resistances of 5, 20, and 40 Ω/□ were prepared by Thin Film Devices, Inc., then cleaned with acetone and isopropanol with ultrasonication for 30 min. The hole-transport layer of poly(3,4-ethylenedioxythiophene) poly(styrenesulfonate) (PEDOT:PSS) (Clevious PH) was spin-cast to a thickness of ca. 35 nm at 5000 rpm for 40 s. The blended BHJ soluriton was prepared using p-DTS(FBTTh$_2$)$_2$:PC$_{71}$BM at 60/40 weight ratio with an overall concentration of 35 mg mL^{-1} in chlorobenzene with 0.4 vol.% of DIO processing additive. The BHJ solution was stirred at 300 rpm on a 60 °C hotplate overnight, and the prepared solution was annealed at 90 °C before film casting for 15 min. The p-DTS(FBTTh$_2$)$_2$:PC$_{71}$BM BHJ active layer was spin-coated with ca. 100 nm thicknesses. A ratio of donor to fullerene of 60:40 weight ratio gave the best results.[12,13] After spin casting, the films were heated to 80 °C for 10 min to dry residual solvents. Then, the Ca layer was evaporated with a thickness of a 20 nm after which the Al cathode was thermally deposited with thickness of ca. 80 nm. The dimensions of the ITO glass substrate were 1.5 × 1.5 cm and the active area of the cell was 4.5 mm^2. The distance between the contact point and the active area is in the range 2.5–13 mm, depending on the location of the active area. However, the performance of the cell does not change significantly due to the position of the active area.

Measurement and Characterization: For the device measurement, the light source was calibrated using by silicon reference cells with an intensity of 100 mW cm^{-2} (AM 1.5 Global) under solar simulation. The *J–V* curves of the solar cells were measured by a Keithley 2400 Sourcemeter. The cell area was determined by the 4.50 mm^2 aperture during the measurement for accurate PCE values. Measurement of the best cell (5 Ω/□-ITO) with the use of aperture gave PCE = 8.24% compared to the device with 40 Ω/□-ITO (PCE = 5.94%) as shown in Table 1. The EQE was measured using by a QE measurement system (PV measurements, Inc.) after the calibration of a monochromatic power to confirm the J_{SC} values through the *J–V* curves. The surfaces of the films were imaged by AFM (AFM Asylum MFP3D) to characterize the surface morphology of the p-DTS(FBTTh$_2$)$_2$:PC$_{71}$BM BHJ film.

Supporting Information

Supporting Information is available from the Wiley Online Library or from the author.

Acknowledgements

Research at UCSB including the fabrication and testing of solar cells and the measurements and analysis were supported by the Air Force Office of Scientific Research, (AFOSR FA9550-11-1-0063), Dr. Charles Lee, Program Officer. AKKK thanks Agency for Science Technology and Research (A*STAR) of Singapore for a postdoctoral fellowship. VG thanks financial support from Indo-US Science and Technology Forum (IUSSTF), Award No. Indo-US Research Fellowship/ 2012-2013/ 26-2012.

Received: March 11, 2013
Published online:

[1] G. Yu, J. Gao, J. C. Hummelen, F. Wudl, A. J. Heeger, *Science* **1995**, *270*, 1789.
[2] G. Li, V. Shrotriya, J. Huang, Y. Yao, T. Moriarty, K. Emery, Y. Yang, *Nat. Mater.* **2005**, *4*, 864.
[3] S. H. Park, A. Roy, S. Beaupré, S. Cho, N. Coates, J. S. Moon, D. Moses, M. Leclerc, K. Lee, A. J. Heeger, *Nat. Photon*, **2009**, *3*, 297.
[4] H.-Y. Chen, J. Hou, S. Zhang, Y. Liang, G. Yang, Y. Yang, L. Yu, Y. Wu, G. Li, *Nat. Photonics* **2009**, *3*, 649.
[5] D. H. Wang, D. Y. Kim, K. W. Choi, J. H. Seo, S. H. Im, J. H. Park, O O. Park, A. J. Heeger, *Angew. Chem., Int. Ed.* **2011**, *50*, 5519.
[6] Z. He, C. Zhong, S. Su, M. Xu, H. Wu, Y. Cao, *Nat. Photonics* **2012**, *6*, 591.
[7] L. Dou, J. You, J. Yang, C.-C. Chen, Y. He, S. Murase, T. Moriarty, K. Emery, G. Li, Y. Yang, *Nat. Photonics* **2012**, *6*, 180.
[8] D. H. Wang, J. K. Kim, J. H. Seo, I. Park, B. H. Hong, J. H. Park, A. J. Heeger *Angew. Chem., Int. Ed.* **2013**, *52*, 2874.

[9] Y. Sun, G. C. Welch, W. L. Leong, C. J. Takacs, G. C. Bazan, A. J. Heeger, *Nat. Mater.* **2012**, *11*, 44.
[10] C. J. Takacs, Y. Sun, G. C. Welch, L. A. Perez, X. Liu, W. Wen, G. C. Bazan, A. J. Heeger, *J. Am. Chem. Soc.* **2012**, *134*, 16597.
[11] J. J. Jasieniak, B. B. Y. Hsu, C. J. Takacs, G. C. Welch, G. C. Bazan, D. Moses, A. J. Heeger, *ACS Nano* **2012**, *6*, 8735.
[12] A. K. K. Kyaw, D. H. Wang, V. Gupta, J. Zhang, S. Chand, G. C. Bazan, A. J. Heeger, *Adv. Mater.* DOI: 10.1002/adma.201300295.
[13] T. S. van der Poll, J. A. Love, T.-Q. Nguyen, G. C. Bazan, *Adv. Mater.* **2012**, *24*, 3646.
[14] B. Walker, A. B. Tamayo, X.-D. Dang, P. Zalar, J. H. Seo, A. Garcia, M. Tantiwiwat, T.-Q. Nguyen, *Adv. Funct. Mater.* **2009**, *19*, 3063.
[15] S. Kim, J. Yim, X. Wang, D. D. C. Bradley, S. Lee, J. C. deMello, *Adv. Funct. Mater.* **2010**, *20*, 2310.
[16] M. W. Rowell, M. A. Topinka, M. D. McGehee, H.-J. Prall, G. Dennler, N. S. Sariciftc, L. Hu, G. Grune, *Appl. Phys. Letts.* **2006**, *88*, 233506.
[17] C. X. Guo, G. H. Guai, C. M. Li, *Adv. Energy Mater.* **2011**, *1*, 448.
[18] C.-L. Hsu, C.-T. Lin, J.-H. Huang, C.-W. Chu, K.-H. Wei, L.-J. Li, *ACS Nano* **2012**, *6*, 5031.
[19] Z. Liu, J. Li, Z.-H. Sun, G. Tai, S.-P. Lau, F. Yan, *ACS Nano* **2012**, *6*, 810.
[20] Y. Xia, K. Sun, J. Ouyang, *Adv. Mater.* **2012**, *24*, 2436.
[21] D. Alemu, H.-Y Wei, K.-C. Ho, C.-W. Chu, *Energy Environ. Sci.* **2012**, *5*, 9662.
[22] M. Vosgueritchian, D. J. Lipomi, Z. Bao, *Adv. Funct. Mater.* **2012**, *22*, 421.
[23] L. A. A. Pettersson, L. S. Roman, O. Inganas, *J. Appl. Phys.* **1999**, *86*, 487.